PCCP

PAPER

View Article Online
View Journal | View Issue

Cite this: *Phys. Chem. Chem. Phys.*, 2014, **16**, 7602

Incidence energy dependent state-to-state time-of-flight measurements of NO(v = 3) collisions with Au(111): the fate of incidence vibrational and translational energy†

Kai Golibrzuch,[ab] Pranav R. Shirhatti,[ab] Igor Rahinov,[c] Daniel J. Auerbach,[abd] Alec M. Wodtke[abd] and Christof Bartels*[ab]

Received 11th December 2013,
Accepted 24th February 2014

DOI: 10.1039/c3cp55224a

www.rsc.org/pccp

We report measurements of translational energy distributions when scattering NO(v_i = 3, J_i = 1.5) from a Au(111) surface into vibrational states v_f = 1, 2, 3 and rotational states up to J_f = 32.5 for various incidence energies ranging from 0.11 eV to 0.98 eV. We observed that the vibration-to-translation as well as the translation-to-rotation coupling depend on translational incidence energy, E_I. The vibration-to-translation coupling, *i.e.* the additional recoil energy observed for vibrationally inelastic (v = 3 → 2, 1) scattering, is seen to increase with increasing E_I. The final translational energy decreases approximately linearly with increasing rotational excitation. At incidence energies E_I > 0.5 eV, the slopes of these dependencies are constant and identical for the three vibrational channels. At lower incidence energies, the slopes gradually approach zero for the vibrationally elastic channel while they exhibit more abrupt transitions for the vibrationally inelastic channels. We discuss possible mechanisms for both effects within the context of nonadiabatic electron–hole pair mediated energy transfer and orientation effects.

1. Introduction

Great strides in our understanding of surface chemistry have been made over the last two decades due to constantly improving computational methods that rely on the Born–Oppenheimer (electronically adiabatic) approximation[1] and exploit the power of modern electronic structure theory, especially density functional theory. Despite this progress, describing and understanding the atomic-scale motion involved in surface reactions remains a daunting challenge.

A central difficulty derives from our lack of understanding of energy exchange between an adsorbate and elementary excitations of the solid. When a molecule with a certain vibrational and translational energy collides with a metal surface, translation and vibration can, in principle, couple to one another or to other degrees of freedom (DOFs) present at the gas–solid interface, *e.g.* molecular rotation, phonon or electron–hole pair (EHP) excitation. State resolved molecular beam scattering under well-defined conditions (ultra-high vacuum, flat single crystal surface *etc.*) using laser-based detection and preparation methods (REMPI, LIF, SEP, SRP, IR overtone excitation *etc.*) has proven to be a powerful tool for investigating the different pathways for energy dissipation.[2]

Experimentalists and theorists have intensively studied NO scattering from various metal surfaces and we now have a good understanding of many features of the energy transfer dynamics of this system. NO scattering from Ag(111) revealed nonadiabatic coupling of thermally excited EHP excitations to vibrational excitation, evidence for which was found in the Arrhenius surface-temperature dependence of the vibrational excitation probabilities.[3,4] Studies focused on the NO/Au(111) system include observations of vibrationally promoted electron transfer,[5] multi-quantum vibrational relaxation and excitation,[5–9] and observation of the effect of NO orientation on the probability of vibrational relaxation.[10] This body of work has revealed certain features of the energy transfer dynamics; most importantly, NO vibrational energy transfer on metals is now believed to be electronically nonadiabatic. That is, the vibration couples to the solid's electrons rather than to phonons, molecular translation or rotation as one might expect from a mechanical (electronically adiabatic) model. The strength of the coupling between vibration and the solid's electronic DOFs depends on translational incidence energy[3,4,6,11,12] and on the orientation of the molecule at the instant of its collision with the surface.[10,13]

[a] *Institute for Physical Chemistry, Georg-August University of Göttingen, Göttingen, Germany*
[b] *Max Planck Institute for Biophysical Chemistry, Göttingen, Germany. E-mail: christof.bartels@mpibpc.mpg.de*
[c] *Department of Natural Sciences, The Open University of Israel, Raanana, Israel*
[d] *Department of Chemistry and Biochemistry, University of California, Santa Barbara, USA*

† Electronic supplementary information (ESI) available. See DOI: 10.1039/c3cp55224a

The experiments have motivated a great deal of theoretical work. Most approaches described the coupling of electronic and vibrational motion in reduced dimensions.[12,14,15] Only recently have higher-dimensional theories become available, where molecular rotation, phonon excitation and three dimensional molecular translation are described from first principles.[13,16,17] Semi-quantitative agreement for vibrational relaxation[13] and excitation[6] probabilities was obtained. Recently, doubts have been raised about the accuracy of the DFT-based interaction potentials used in this approach.[11] This points out the need to compare the predictions of new high-dimensional theories to more sophisticated state-to-state experiments that probe more DOFs than just vibration and translation.

Other systems where nonadiabatic vibrational energy transfer has been observed are NO/Cu(110)[18] and HCl/Au(111).[19] The collision-induced NO vibrational excitation in scattering from Cu(110) shows similar features found for NO/Ag(111) and NO/Au(111).

Studies on the dependence of final translational energy on the final quantum state are quite limited. Kimman *et al.* investigated the energy transfer from initial translational to final rotational and phonon excitation for NO(v = 0) scattering from Ag(111).[20,21] They found that molecules that underwent rotational excitation were scattered with higher translational energy than expected from simple energy conservation considerations taking into account only translational and rotational degrees of freedom of the impinging molecule. With the help of molecular dynamics simulations, the authors were able to interpret their observations in terms of an anti-correlation between translational energy transfer to rotation and to phonons. In other words, collisions that lead to large rotational excitation tend to produce reduced phonon excitation.

Other studies on translation-to-rotation coupling did not directly measure the kinetic energy of scattered molecules.[22–24] For example, for the NO(v = 0)/Ag(111) system Geuzebroek *et al.* showed that the final rotational excitation depends strongly on the orientation of the NO molecules,[22] a result that was also seen for scattering of vibrationally excited molecules.[10]

Only recently have the first measurements of coupling between vibration and translation (V → T and T → V coupling) been reported for NO scattering from a metal.[25] Prior to this work, it was assumed that translation was a spectator to energy exchange between molecular vibration and the electronic DOFs of the solid. In ref. 25, V → T and T → V couplings were measured to be ∼12% of the vibrational energy transferred. That work was restricted to a single incidence energy of translation (E_I = 0.65 eV), but investigated a large number of vibrational state-to-state scattering channels, both in excitation and in relaxation. The coupling between vibration and translation was also found to be surface temperature dependent.

In this paper, we present results of a detailed study on the translation-to-rotation (T → R) and V → T coupling for NO(v_i = 3, J_i = 1.5) colliding with a single crystal Au(111) surface. We extend the results of ref. 25 by systematically examining the incidence translational energy dependence of these quantities. We apply a previously introduced IR-UV double resonance technique, which enables us to measure high resolution state-to-state time-of-flight spectra.[25,26] From such data, we can extract the velocity and translational energy distributions of molecules scattered into specific ro-vibrational states. This approach enables us to map out the amount of internal energy that is lost to the surface during the collision. Our results show that the V → T coupling strongly depends on incidence energy, E_I. We also find that at high E_I, the dependence of final translational energy on the final rotational energy ($\Delta E_f/\Delta E_{rot}$) is the same for all three final vibrational states, v = 3 → 3, 2, 1. However, as E_I is lowered $\Delta E_f/\Delta E_{rot}$ becomes strongly dependent on the final vibrational state, *i.e.* the vibrationally inelastic (v = 3 → 2, 1) channels behave differently than the vibrationally elastic (v = 3 → 3) channel.

None of these observations has been previously predicted by theory. Therefore these data stand as an interesting comprehensive benchmark for the testing of new theories of electronically nonadiabatic energy transfer of molecules at metal surfaces.

2. Experimental

The experimental set-up has been described earlier in detail.[27] Briefly, we generate a pulsed molecular beam (FWHM ∼ 70 μs) by supersonic expansion of a gas mixture through a piezo-electrically driven nozzle at 3 bar stagnation pressure. We produce NO incident translational energies from 0.11 to 0.98 eV by seeding different amounts of NO in H_2 or N_2. The beam passes two stages of differential pumping through a skimmer and apertures and enters an ultra-high vacuum (UHV) chamber (2×10^{-10} Torr base pressure, 2×10^{-9} Torr with the molecular beam operating). The beam encounters a Au(111) single crystal at near normal incidence (∼2–3°). An ion detector consisting of an ion lens and a micro-channel plate (MCP) detector stands in close proximity to the gold sample. Prior to every experiment, we clean the crystal using Ar^+ bombardment (3 keV) for 20 minutes, followed by 30 minutes annealing at 1000 K to recover the (111) surface configuration. Auger electron spectroscopy monitors the cleanliness of the sample.

We apply (1+1) resonance enhanced multiphoton ionization (REMPI) detection *via* the $\tilde{A}^2\Sigma^+$ state using the output of a frequency doubled dye laser (0.1 cm^{-1} bandwidth) for state specific detection of NO. More specifically, we use the $\tilde{A}^2\Sigma^+$ (v = 0) ← $\tilde{X}^2\Pi_r$ (v = 1, 2) and $\tilde{A}^2\Sigma^+$ (v = 1) ← $\tilde{X}^2\Pi_r$ (v = 3) bands in the range from 235 nm to 250 nm for detection of NO(v = 1, 2, 3), respectively. Note that due to the complicated rotational structure of the $\tilde{A}$ ← $\tilde{X}$ bands, many rotational lines are blended or overlapped. Therefore, only transitions with clearly resolved rotational quantum numbers were chosen to monitor the translational energies of the scattered NO molecules.

For preparation (tagging) of incident NO molecules in v_i = 3, J_i = 1.5, we use a recently introduced high power IR laser system with Fourier transform limited bandwidth to pump the 3 ← 0 R(0.5) transition at 5548.875 cm^{-1}.[25] A single mode cw ring dye laser (669 nm, 400 mW) is used for seeding a 5-stage pulse

amplifier pumped by the second harmonic of an injection-seeded Nd:YAG laser. IR radiation is generated by difference frequency mixing of the pulse amplified light and the fundamental of the injection-seeded Nd:YAG laser resulting in IR light at a wavelength of ~1.8 μm (pulse energy 3–5 mJ). The IR pulses are further amplified in an OPA process producing signal (1.8 μm, up to 30 mJ) and idler wavelengths (2.6 μm, up to 20 mJ) with ~130 MHz bandwidth.

Experiments are performed with the geometries shown in Fig. 1. Both the REMPI and IR laser beams can be translated parallel and perpendicular to the incident molecular beam. Fig. 1a shows the geometry used to measure the molecular beam velocity distribution. Here, we move the surface up by 10 mm to get it out of the beam path. The IR laser excites the incident NO molecules *via* the $3 \leftarrow 0$ $R(0.5)$ transition. The REMPI laser is positioned 30 mm downstream to detect the excited NO($v = 3, J = 1.5$) molecules. We scan the temporal delay of the REMPI laser with respect to the IR laser to measure time-of-flight spectra. The characteristics of all molecular beams are given in Table 1.

Fig. 1b shows the geometry used to make state-specific TOF measurements of scattered NO molecules. Here, the IR laser is focused using a 750 mm lens about 1 mm in front of the surface.

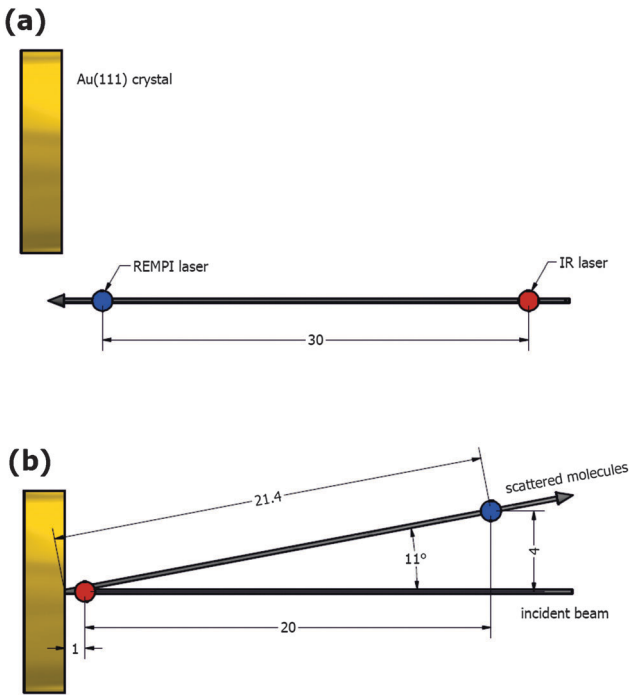

Fig. 1 Experimental set-up for measurement of state-to-state time-of-flight spectra. (a) For determination of the translational energy distribution of the incoming molecular beam we move the surface up by about 10 mm in order to avoid any scattering. The IR laser is positioned 30 mm upstream from the REMPI beam. (b) Set-up for measurement of scattered energy distributions. Incident NO molecules are excited (tagged) *via* the $3 \leftarrow 0$ R(0.5) transition less than 1 mm in front of the surface. The exact distance is measured prior to every experiment. The REMPI beam is placed 20 mm away from the IR laser with a vertical offset of 4 mm which corresponds to an angle of about 11°. The vertical offset is necessary to avoid non-resonant 2-photon ionization background from the intense incident beam.

Table 1 Characteristics of the incident molecular beams used in this work. The incident velocity distribution is represented by a function of the form $\varphi_i(s) = A{\cdot}s^3\exp[-(s - s_0)^2/\alpha_0{}^2]$. The distribution is fully characterized by the velocity S_0 and the width parameter α_0

Mixing ratio	s_0 (m s^{-1})	α_0 (m s^{-1})	$\langle s \rangle$ (m s^{-1})	FWHM (m s^{-1})	$\langle E \rangle$ (eV)	FWHM (eV)
10% NO/90% N_2	826	51	831	85	0.11	0.02
6% NO/24% N_2/70% H_2	1296	84	1304	139	0.27	0.06
15% NO/85% H_2	1563	98	1572	163	0.39	0.08
10% NO/90% H_2	1750	62	1754	103	0.48	0.06
9% NO/91% H_2	1824	81	1829	135	0.52	0.08
7% NO/93% H_2	1908	186	1935	308	0.58	0.18
6.5% NO/93.5% H_2	2016	71	2020	119	0.64	0.07
2% NO/97% H_2	2310	104	2317	172	0.84	0.12
1% NO/98% H_2	2505	112	2513	186	0.98	0.14

The distance (d_1) from the Au(111) surface is measured prior to every measurement by translating the surface towards the IR laser beam and monitoring the transmitted intensity. The REMPI detection laser is displaced 20 mm parallel and 4 mm perpendicular to the beam direction. This leads to an effective flight distance from surface to ionization of 21.4 mm, assuming that the IR laser is 1 mm from the surface. In order to improve our temporal resolution, we focus the REMPI beam using a 500 mm CaF_2 lens. However, we work slightly off the focus to minimize the background from non-resonant two photon ionization. We scan the temporal delay of the REMPI laser with respect to the IR laser to measure time-of-flight spectra like those shown in Fig. 2. The time-of-flight profiles for NO($v = 3 \rightarrow 1$) are recorded with and without the IR laser to correct for influences of NO($v = 1$) present in the molecular beam. The total time t that the tagged molecules need until they arrive at the detection laser can be divided into the time $t_1 = d_1/\langle s_i \rangle$ between the IR tagging and the surface collision, and the time $t_2 = d_2/\langle s_{scattered} \rangle$ between the surface collision and the laser ionization (assuming negligibly small residence times).

3. Results

We measured state-to-state time-of-flight spectra like those shown in Fig. 2 for incidence energies of 0.26, 0.65 and 0.98 eV. Here, incident NO($v_i = 3, J_i = 1.5$) scatters into various rotational and vibrational states upon collision with the Au(111) surface. The investigated rotational energies range from less than 1 meV ($J_f = 3.5, 5.5$) up to 0.23 eV for $J_f = 32.5$. The vibrational energy loss ranges from zero for $v = 3 \rightarrow 3$ collisions to as large as 0.47 eV for $v = 3 \rightarrow 1$ collisions.

We use forward convolution to model the observed distributions, taking into account the incident beam velocity distribution represented by $\varphi_i(s) = As^3\exp[-(s - s_0)^2/\alpha_0{}^2]$, where φ represents the flux, A is a normalization constant, s is the speed and s_0 and a_0 are parameters that describe the most probable speed and the width of the distribution, respectively. The speed distribution of scattered molecules is described by a flowing Maxwell–Boltzmann distribution, $\varphi_f(s,s_i) = As^3\exp[-(s - \gamma s_i)^2/\alpha^2]$, where s_i is the speed of the incident molecule, γ describes the most probable speed of scattered molecules as a fraction of s_i,

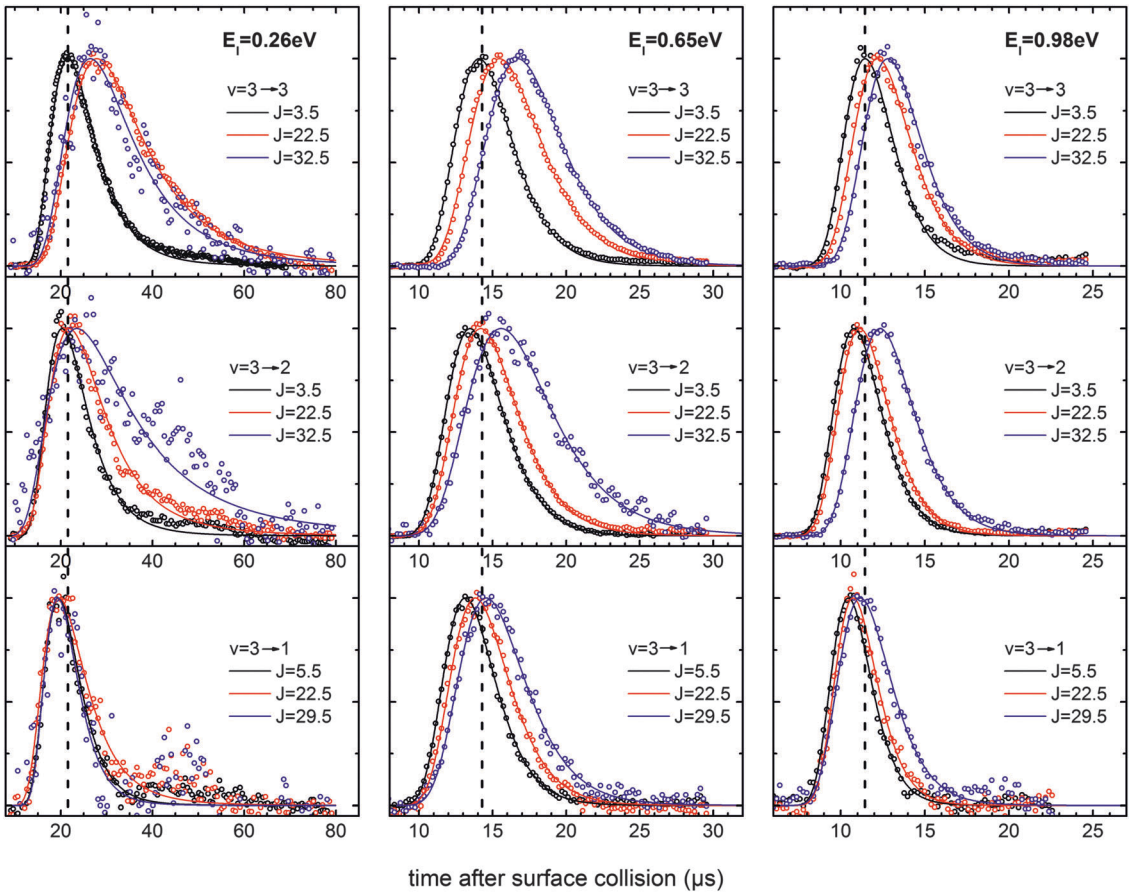

Fig. 2 State-to-state time-of-flight spectra observed for NO(v_i = 3, J_i = 1.5) scattering into different vibrational and rotational states for incidence energies of 0.26 eV (left column), 0.65 eV (middle column) and 0.98 eV (right column). The vertical dashed lines are drawn through the peaks of the vibrationally elastic (v = 3 → 3) and rotationally quasi-elastic (J_f = 3.5, 5.5) experimental distributions to guide the eye. Upper panels: vibrationally elastic scattering into v_f = 3 and J_f = 3.5, 22.5, 32.5. We clearly observe longer flight times for higher rotational states corresponding to lower translational energies. Middle panels: vibrationally inelastic scattering into v_f = 2 and J_f = 3.5, 22.5, and 32.5. Again higher rotational states arrive later at the detection laser. Furthermore, the time-of-flight spectra are overall shifted towards earlier arrival times than the vibrationally elastic channels. Lower panels: vibrationally inelastic scattering into v_f = 1 for J_f = 5.5, 22.5, 29.5. Overall the molecules show earlier arrival times than seen in 3 → 3 and 3 → 2 scattering whereas increasing rotational energy leads to longer flight times. Note that this effect almost vanishes in the data for 0.26 eV incidence energy. The second peak near t = 50 μs for the 3 → 1 channel at E_i = 0.26 eV is attributed to an artifact originating from the background correction.

and α describes the width of the distribution. We use Jacobians and flux-to-density conversion to convert $\varphi_f(s,s_i)$ into an arrival time distribution as measured by a density detector. Further we assume that we ionize and detect all molecules along the REMPI beam with the same probability, and that the angular distributions do not change significantly with J. We use angular distributions from ref. 7 to correct for this effect. A detailed description of the procedure is given in ref. 25.

The fits to the time-of-flight data shown in Fig. 2 faithfully describe the measured data set. The translational energy distributions derived from these fits are presented in Fig. 3. The corresponding incident translational energy distributions are shown as dashed gray lines. The reader is directed to take note of a number of simple features of the analysis.

First, the scattered molecules lose a large fraction of their incident kinetic energy to the surface. The vertical lines in Fig. 3 indicate the recoil energies predicted by a simple hard cube model, often referred to as the Baule limit.[28] In this model, the expected final translational energies, $\langle E_f \rangle$, can be calculated from conservation of energy and momentum using the relation $\langle E_f \rangle = \langle E_i \rangle \left(\frac{m_{Au} - m_{NO}}{m_{Au} + m_{NO}} \right)^2$. We find quite good agreement of this hard cube limit for vibrationally elastic (v_f = 3) and rotationally quasi-elastic (J_f = 3.5) scattering, which is the only scattering channel where a reasonable comparison to this model should be made since the hard cube model does not include internal DOFs (rotation, vibration). Second, in general for the complete data set, increased rotational excitation is correlated with lower final translational energies in vibrationally elastic scattering (top panels). Third, for vibrationally inelastic scattering with loss of one (middle panels) and two vibrational quanta (lower panels) we find a slight shift towards higher kinetic energies in comparison to the vibrationally elastic channel for all three incidence energies. Fourth, for vibrationally and rotationally inelastic scattering we find that the final translational energy decreases with increasing J_f,

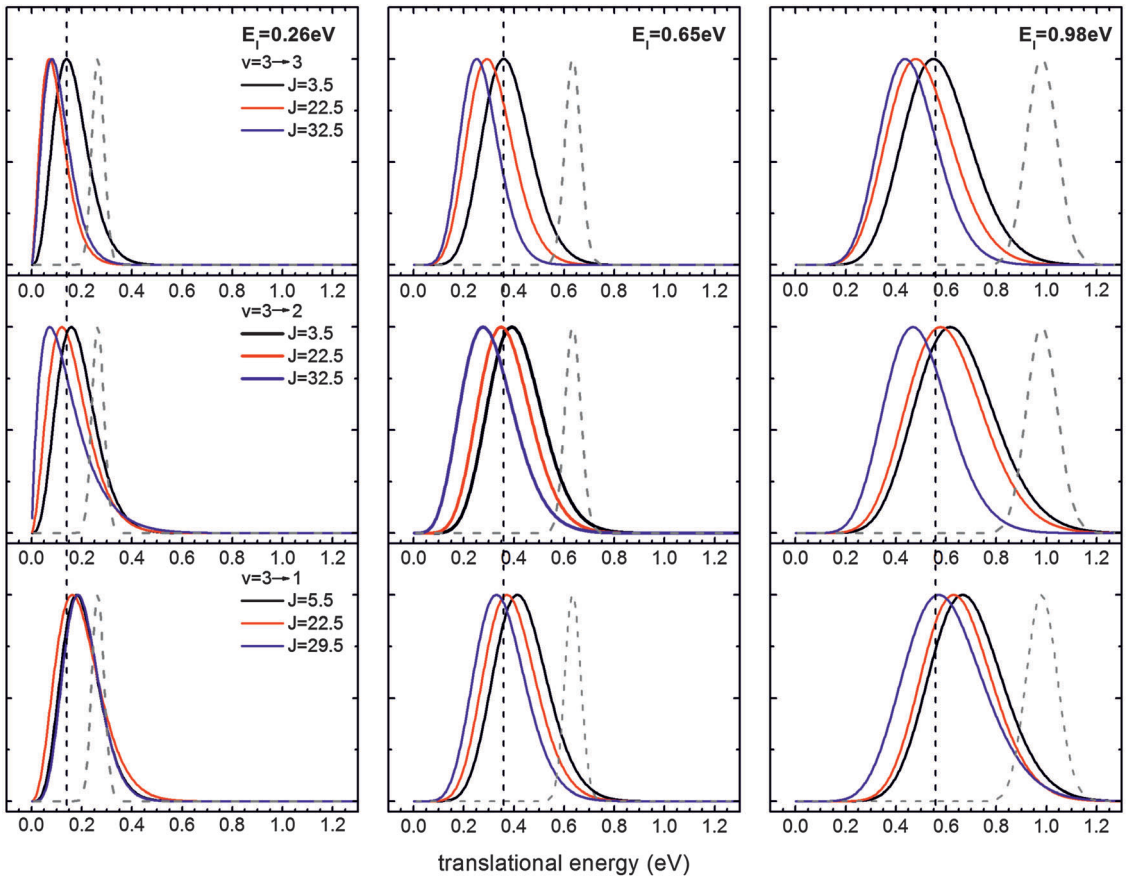

Fig. 3 Fits to the time-of-flight distribution from Fig. 2 (same color scheme) converted into energy space. In all panels the dashed gray curves represent the kinetic energy distributions of the corresponding incident molecular beam. It appears that the scattered energy distributions are clearly broadened with respect to the incident beam. This effect can be related to the thermal motion of the surface atom (see ref. 25 for details). Furthermore we observe that the molecules lose about half of their initial kinetic energy to the surface for J_f = 3.5, 5.5 ($E_{rot} < 1$ meV). Higher rotational states are scattered even slower at E_I = 0.65 eV and 0.98 eV. The effect becomes smaller in the left panels (E_I = 0.26 eV) especially for the loss of two vibrational quanta, where the differences become insignificant.

except for $v_f = 1$ and $E_I = 0.26$ eV (lower left panel) where this effect is absent.

To show some of these effects more clearly, we present the mean final translational energies $\langle E_f \rangle$ as a function of final rotational excitation and final vibrational states in Fig. 4. A large amount of data, similar to that shown in Fig. 2, was obtained for nine initial translational energies ranging from 0.11 eV to 0.98 eV and final rotational energies from 0 to 0.23 eV (see ESI† for details of the corresponding speed and energy distributions). We observe an approximately linear relationship between scattered translational and rotational energy over the entire range of rotational energies studied here. This observation holds for vibrationally elastic and inelastic scattering; however, we find that the slope of the linear relationship depends critically on E_I and v_f. Specifically, it approaches zero for vibrationally inelastic channels at low E_I.

Although weaker, this effect is also observed for vibrationally elastic NO($v = 3 \rightarrow 3$) scattering. Furthermore, Fig. 4 makes clear that vibrational relaxation leads to an increase in outgoing translational energy for all incidence translational energies studied here. We note that the pure vibration-to-translation (V → T) coupling, which we extract from an extrapolation to $E_{rot} = 0$, depends strongly on incidence translational energy. For example, we find that loss of two vibrational quanta ($3 \rightarrow 1$) at $E_I = 0.98$ eV leads to an increase in $\langle E_f \rangle$ of 124 meV whereas only an increase of 25 meV is observed for $E_I = 0.26$ eV.

4. Discussion

We now discuss the possible origins of the observations reported above. This section is organized as follows. First we will discuss the mechanical excitation of the solid (phonons), before we focus on the vibrational-to-translation energy transfer and afterwards on the dependence of final translation on the amount of rotational excitation for vibrationally elastic and inelastic scattering.

4.1. Energy loss to the solid

As illustrated in Fig. 5, the NO molecules always lose about half their translational energy when colliding with the Au(111) surface. The open symbols are found from linear extrapolation

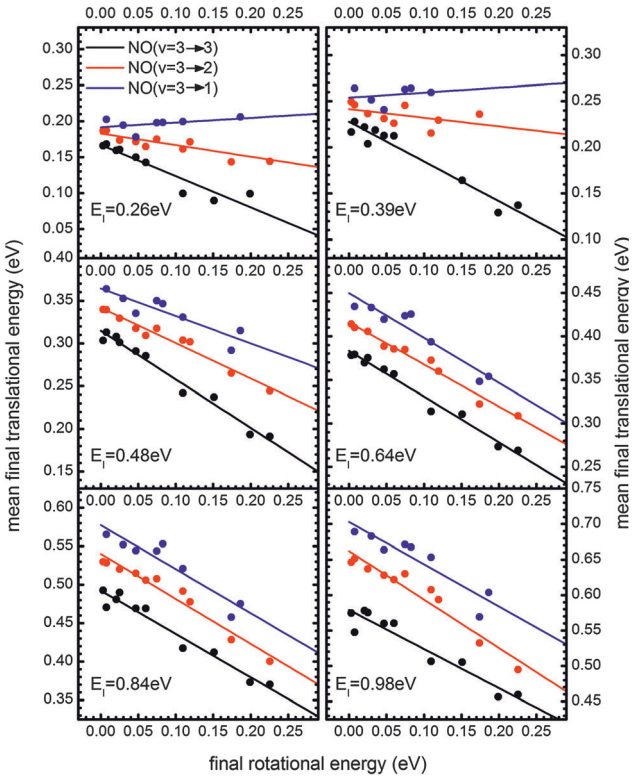

Fig. 4 Mean final translational energy of the scattered molecules as a function of final rotational energy for six different incidence energies from 0.26 eV to 0.98 eV for $v = 3 \rightarrow 3$ (black), $v = 3 \rightarrow 2$ (red) and $v = 3 \rightarrow 1$ (blue) scattering. At high incidence kinetic energies (0.65–0.98 eV) we observe similar slopes $\Delta E_f/\Delta E_{rot}$ for all vibrational scattering channels. At $E_I = 0.48$ eV, the slopes for vibrationally inelastically scattered molecules ($v = 3 \rightarrow 2$, $v = 3 \rightarrow 1$) start to deviate from the vibrationally elastic channel. This effect is even more pronounced for $E_I = 0.41$ eV and 0.26 eV, where the final translational energy becomes almost independent (within experimental uncertainty) of the final rotational state for $v = 3 \rightarrow 1$ scattering, and approaches $\Delta E_f/\Delta E_{rot} = 0$ for $v = 3 \rightarrow 2$ scattering.

of the mean final translational energy shown in Fig. 4 to zero rotational energy as well as the same analysis applied to the most probable final translational energy E_f^{MP}.

The prediction of a simple hard cube model (dashed curve), with an impinging hard sphere representing the NO molecule ($m_{NO} = 30$ amu) colliding with an isolated hard cube representing the Au atom ($m_{Au} = 197$ amu) – often referred to as the Baule limit[28] – is close to but systematically below the experimental results. This indicates that the effective mass of the surface is somewhat bigger than the mass of a single Au atom. The fact that the scattered translational energy "remembers" the incidence translational energy and that it is in rough agreement with the Baule model indicates that trapping/desorption does not influence the observations. Under our conditions, $k_B T_S = 0.026$ eV (dotted line) is a measure of the expected translational energy for molecules that undergo trapping/desorption. Even at the lowest incidence energies, the observed translational energies of the scattered molecules exceed this value. We conclude that the observations of this work reflect direct scattering dynamics.

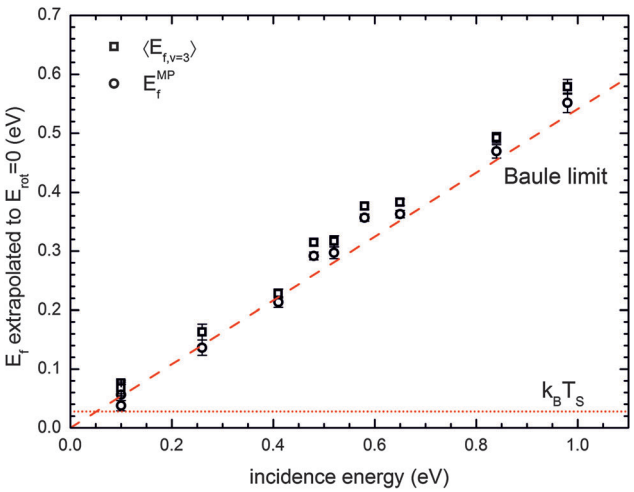

Fig. 5 Mean translational energy $\langle E_f \rangle$ (open squares) and the most probable translational energy E_f^{MP} (open circles) from a linear extrapolation of the data shown in Fig. 4 to $E_{rot} = 0$ for vibrationally elastic NO($v = 3 \rightarrow 3$) scattering. The dashed red line shows the expectation of a simple hard cube model (Baule limit), the red dotted line the expected mean kinetic energy at the surface temperature of $T_s = 320$ K.

4.2. Vibration-to-translation energy transfer

There is now considerable experimental evidence that vibrational excitation and de-excitation in NO collisions with Au and Ag surfaces are due to the nonadiabatic coupling to the electron–hole pairs in the metal.[3–6,8,9,29–33] In such a strongly electronically nonadiabatic system, translational motion was historically considered a spectator to the vibrational energy transfer.[12,14] While increased incidence energy of translation can increase the nonadiabatic coupling strength, it was thought to not directly exchange energy with the vibrational DOF. Recently, we have shown that this view is only approximately true.[25] We found that molecules that became vibrationally excited were scattered slower, whereas those molecules that were vibrationally de-excited gained a certain amount of translational energy. Moreover, that study revealed that the amount of observed T–V coupling depends on the surface temperature. That work was, however, restricted to a single incidence energy of translation, 0.62 eV.

Here, we extend our work to a much larger range of incidence energies. In contrast to the previous study, we use a constant surface temperature of $T_S = 320$ K. Under these conditions we observe only vibrational relaxation and essentially no vibrational excitation. We extract the pure V → T energy transfer, $\langle E_{f,v=2,1} \rangle - \langle E_{f,v=3} \rangle$, by linear extrapolation of the mean translational energies (Fig. 4) for each channel to $E_{rot} \rightarrow 0$.

The derived vibrational energy release appearing as outgoing translational motion is shown in Fig. 6. We find that the amount of vibrational energy channeled into translation increases with incidence energy of translation. This result is starkly different from previously reported results for HCl($v = 2 \rightarrow 2,1$)/Au(111) where a constant fraction of 26% of the vibrational energy is channeled into translation for incidence energies ranging from 0.1 to 1.27 eV.[26] Note that for NO/Au(111) scattering the (absolute) amount of vibrational energy channeled into translation is

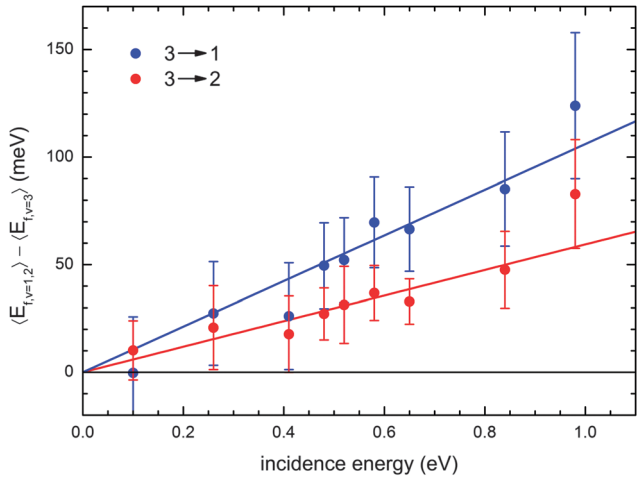

Fig. 6 The $\langle E_{f,v=2,1}\rangle - \langle E_{f,v=3}\rangle$ energy difference (V → T energy transfer) based on a linear extrapolation to E_{rot} = 0 of the data shown in Fig. 4. Error bars are taken from the linear fits in Fig. 4 using 90% confidence interval. The figure shows how much translational energy the scattered molecules gain with respect to the vibrationally elastic v = 3 → 3 channel when they lose one (red dots) or two quanta (blue dots) of vibration (in the case of rotationally elastic scattering). We find that the vibrational energy released into translation is 0–10 meV at the lowest incidence energy of 0.1 eV, increasing with E_i to 80 meV (34% of ΔE_{vib}) for loss of one vibrational quantum and to 120 meV (26% of ΔE_{vib}) for loss of two quanta at E_i = 0.98 eV.

approximately twice as large for relaxation of two quanta as it is for relaxation of one quantum of vibration, *i.e.* the fractions are similar.

We are not aware of a theoretical prediction of this kind of behavior. A number of speculative explanations could be suggested including: (1) image charge acceleration due to transient NO^- formation, (2) a "mixed" adiabatic/nonadiabatic behavior where a part of the vibrational energy loss is channeled into outgoing translation or (3) V–T coupling mediated by EHPs.

The first two mechanisms do not seem capable of explaining why the V–T coupling should increase with incidence energy of translation or with surface temperature.[25] Only the third mechanism holds out hope for being able to explain our observations. In this picture, vibrational relaxation energy is first transferred to the electronic system of the metal which then couples to translation (hot electron to translation coupling). In vibrational excitation, energy is removed from the hot EHP bath and this is compensated by loss of some translational energy of the molecule. Pursuing this idea further, we speculate that for increasing incidence energy of translation, the NO molecule can penetrate into regions of higher electron density, leading to a stronger coupling of the EHPs to vibration and translation and hence to higher EHP-mediated V–T coupling.

4.3. Dependence of $\langle E_f\rangle$ on final rotational and vibrational energy

Fig. 4 shows the observed (approximately linear) relationship between final translational, E_f, and rotational, E_{rot}, energy of the scattered NO molecules for each of the three vibrational channels and for six incidence energies of translation studied in this work. Specifically, we have plotted the average value, $\langle E_f\rangle$, obtained for each final rotational state. The slope of a best fit line, $d\langle E_f\rangle/dE_{rot}$, which is obtained separately for each incidence energy and for each vibrational channel, reflects the relationship of translational energy transfer to rotation and to phonons.

The meaning of different values of $d\langle E_f\rangle/dE_{rot}$ has been given previously[20] but will be recalled here. We note two simple limiting cases: First, $d\langle E_f\rangle/dE_{rot} \rightarrow -1$ indicates pure energy conservation for translation-to-rotation (T → R) energy transfer, *i.e.* $E_f + E_{rot}$ = constant, while the energy transferred to the surface (E_{surf}) remains constant irrespective of the final rotational excitation. This would be expected for mechanical T → R coupling in collisions with a stiff surface. Second, $d\langle E_f\rangle/dE_{rot} \rightarrow 0$ indicates that the final rotation and surface excitation are completely (anti-)correlated, $E_{surf} + E_{rot}$ = constant, while the final translational energy is independent of rotational excitation. This corresponds to a situation where the energy for rotational excitation is taken from the surface bath (S → R coupling).

Fig. 7 shows $\Delta\langle E_f\rangle/\Delta E_{rot}$ for each vibrational channel as a function of incidence energy of translation. We find that at high incidence energy $\Delta\langle E_f\rangle/\Delta E_{rot} = -0.6 \pm 0.2$ which is demonstrably greater than the limit −1. This deviation, which is consistent with previous work,[20,34–36] arises because the partitioning of incidence translational energy between phonons and rotation depends on the orientation of the molecule at impact. At low incidence energy in Fig. 7, we see that $\Delta\langle E_f\rangle/\Delta E_{rot}$ approaches 0. For the vibrationally elastic (3 → 3) channel this transition occurs smoothly over the range of incidence energies studied.

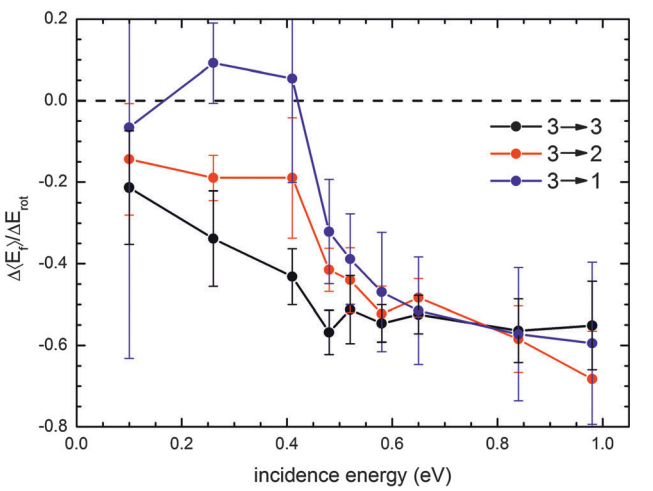

Fig. 7 Values for $\Delta\langle E_f\rangle/\Delta E_{rot}$ obtained from linear fits like those in Fig. 4 as a function of incidence translational energy. The error bars indicate 90% confidence intervals. For vibrationally elastic NO(v = 3 → 3) scattering (black), $\Delta\langle E_f\rangle/\Delta E_{rot}$ stays constant at about −0.55 for incidence energies ranging from 0.98 eV to ≈0.5 eV. At lower incidence energies, it gradually increases to about −0.2 at E_i = 0.1 eV. For vibrationally inelastic NO(v = 3 → 1) (blue) and NO(v = 3 → 2) (red) scattering, $\Delta\langle E_f\rangle/\Delta E_{rot}$ starts to increase already at higher E_i values, and the change is more rapid than for the elastic channel. In the case of NO(v = 3 → 1), the upper limit of 0 is reached already at E_i = 0.41 eV.

Vibrationally inelastic ($3 \rightarrow 2$ and $3 \rightarrow 1$) channels behave similar to vibrationally elastic ($3 \rightarrow 3$) scattering for E_I = 0.6 to 1.0 eV. However they show an abrupt transition to $\Delta\langle E_f\rangle/\Delta E_{rot} \rightarrow 0$ at a switching energy of $E_I \sim 0.4$ eV, below which $\Delta\langle E_{f,v=1,2}\rangle/\Delta E_{rot}$ significantly deviates from $\Delta\langle E_{f,v=3}\rangle/\Delta E_{rot}$.

One possible explanation for this behavior is dynamical steering.[13] Experiments with oriented NO molecules at high incidence energies show that vibrational relaxation is favored when the N-atom is oriented toward the Au(111) surface.[10] Below $E_I \sim 0.3$ eV, the initial orientation becomes irrelevant, meaning that the molecule – regardless of its initial orientation – is re-oriented to an N-first orientation by the forces it experiences on approaching the Au(111) surface. This N–Au attraction could lead to an additional acceleration that preferentially couples phonons to rotation, resulting in $\Delta\langle E_f\rangle/\Delta E_{rot} \rightarrow 0$. The incidence energy at which dynamical steering becomes important[13] is similar to the $\Delta\langle E_f\rangle/\Delta E_{rot}$ switching energy seen here. Therefore it seems reasonable that the change in $\Delta\langle E_f\rangle/\Delta E_{rot}$ is related to a change in (re-)orientation dynamics. Furthermore, this might provide an explanation why the switching behavior is seen most clearly for vibrationally inelastic channels, whereas for the vibrationally elastic channel no switching energy can be identified.

Other possible explanations should also be mentioned. Kimman *et al.*[20] reported the incidence translational energy dependence of $\Delta\langle E_f\rangle/\Delta E_{rot}$ for vibrationally elastic NO($v = 0 \rightarrow 0$) scattering from Ag(111). They analyzed their observations with molecular dynamics simulations using an empirical potential energy surface. At low E_I they found complicated trajectories in the MD simulations which suggested that multi-bounce collisions might play a role in the $\Delta\langle E_f\rangle/\Delta E_{rot} \rightarrow 0$ behavior. It is conceivable that for N-first orientations, where the N–Au attraction is larger, multi-bounce dynamics could be more important for vibrationally inelastic than for vibrationally elastic events. Furthermore, multi-bounce dynamics will increase the interaction time and enhance the vibrational relaxation probability.

On the other hand, several points suggest that multi-bounce dynamics are not important here. Most importantly, the measured translational energies of scattered NO molecules (see for example Fig. 5) show no indication of deviation from the Baule model, which would be expected if there were a transition of single bounce dynamics at high energy to multi-bounce dynamics at low incidence energy. However, we note that the Baule model should not be taken as unambiguous evidence for single-bounce dynamics. However, we find that the hard cube describes NO/Au(111) scattering very well in the high E_I regime in which single-bounce collision should dominate the dynamics.

5. Conclusions

In summary, we have measured a detailed set of translational energy distributions for vibrationally and rotationally elastic and inelastic collisions of incident NO($v_i = 3, J_i = 1.5$) molecules with Au(111). In the limit of rotationally elastic collisions we find that the vibration-to-translation energy transfer, $\Delta\langle E_{f,v=1,2}\rangle - \Delta\langle E_{f,v=3}\rangle$, increases with increasing incidence energy. The mechanism for this energy transfer is still unclear but the E_I dependence suggests an EHP-mediated process that relies on a similar mechanism as observed for vibrational excitation and relaxation probabilities. Furthermore our approach enabled us to study the dependence of final translational energy on the final rotational state for vibrationally elastic and inelastic surface collisions. We found that the slope of the observed $\langle E_f\rangle$-*vs.*-$\langle E_{rot}\rangle$ dependence, $\Delta\langle E_f\rangle/\Delta E_{rot}$, increases from negative values near -0.6 to values near zero with decreasing E_I for all three vibrational channels. However, we found that while this increase is gradual for the vibrationally elastic $3 \rightarrow 3$ channel, there is a much more abrupt change at $E_I \sim 0.4$ eV for vibrationally inelastic $3 \rightarrow 2$ and $3 \rightarrow 1$ scattering. We note that the observed switching energy is quite close to recently observed values of the incidence energy where the dynamical steering of NO by a Au(111) surface shuts down,[10] suggesting that the abrupt change in $\Delta\langle E_f\rangle/\Delta E_{rot}$ observed for the vibrationally inelastic scattering channels is related to a transition in the underlying orientation dynamics.

We hope that this detailed set of experimental data will motivate future theoretical work, which includes all DOFs of the system. Any new theoretical approach that can explain all of the detailed measurements of this work will significantly improve our understanding of electronically nonadiabatic gas–surface interactions.

Acknowledgements

AMW, DJA and CB gratefully acknowledge support from the Alexander von Humboldt foundation.

References

1 M. Born and R. Oppenheimer, Zur Quantentheorie der Molekeln, *Ann. Phys.*, 1927, **389**(20), 457–484.
2 G. O. Sitz, Gas surface interactions studied with state-prepared molecules, *Rep. Prog. Phys.*, 2002, **65**(8), 1165.
3 C. T. Rettner, *et al.*, Observation of direct vibrational-excitation in gas-surface collisions - NO on Ag(111), *Phys. Rev. Lett.*, 1985, **55**(18), 1904–1907.
4 C. T. Rettner, *et al.*, Direct vibrational-excitation in gas surface collisions of NO with Ag(111), *Surf. Sci.*, 1987, **192**(1), 107–130.
5 Y. Huang, *et al.*, Vibrational Promotion of Electron Transfer, *Science*, 2000, **290**(5489), 111–114.
6 R. Cooper, *et al.*, Multiquantum Vibrational Excitation of NO Scattered from Au(111): Quantitative Comparison of Benchmark Data to Ab Initio Theories of Nonadiabatic Molecule–Surface Interactions, *Angew. Chem.*, 2012, **124**(20), 5038–5042.
7 R. Cooper, *et al.*, On the determination of absolute vibrational excitation probabilities in molecule-surface scattering: Case study of NO on Au(111), *J. Chem. Phys.*, 2012, **137**(6), 064705.
8 R. Cooper, *et al.*, Vibrational overtone excitation in electron mediated energy transfer at metal surfaces, *Chem. Sci.*, 2010, **1**(1), 55–61.

9 D. Matsiev, *et al.*, On the temperature dependence of electronically non-adiabatic vibrational energy transfer in molecule-surface collisions, *Phys. Chem. Chem. Phys.*, 2011, **13**(18), 8153–8162.
10 N. Bartels, *et al.*, Observation of orientation-dependent electron transfer in molecule–surface collisions, *Proc. Natl. Acad. Sci. U. S. A.*, 2013, **110**(44), 17738–17743.
11 F. Gratz, *et al.*, Vibrational enhancement of electron emission in CO (a3Pi) quenching at a clean metal surface, *Phys. Chem. Chem. Phys.*, 2013, **15**(36), 14951–14955.
12 D. M. Newns, Electron-hole pair mechanism for excitation of intramolecular vibrations in molecule-surface scattering, *Surf. Sci.*, 1986, **171**(3), 600–614.
13 N. Shenvi, S. Roy and J. C. Tully, Dynamical Steering and Electronic Excitation in NO Scattering from a Gold Surface, *Science*, 2009, **326**(5954), 829–832.
14 G. Ertl, Elementary Steps in Heterogeneous Catalysis, *Angew. Chem., Int. Ed. Engl.*, 1990, **29**(11), 1219–1227.
15 S. Monturet and P. Saalfrank, Role of electronic friction during the scattering of vibrationally excited nitric oxide molecules from Au(111), *Phys. Rev. B: Condens. Matter Mater. Phys.*, 2010, **82**(7), 075404.
16 S. Roy, N. A. Shenvi and J. C. Tully, Model Hamiltonian for the interaction of NO with the Au(111) surface, *J. Chem. Phys.*, 2009, **130**(17), 174716.
17 J. H. Moore, C. C. Davis and M. A. Coplan, *Building scientific apparatus: a practical guide to design and construction*, 1989, Addison-Wesley, Advanced Book Program.
18 E. U. Condon, The Franck-Condon Principle and Related Topics, *Am. J. Phys.*, 1947, **15**(5), 365–374.
19 Q. Ran, *et al.*, Observation of a change of vibrational excitation mechanism with surface temperature: HCl collisions with Au(111), *Phys. Rev. Lett.*, 2007, **98**(23), 237601.
20 J. Kimman, *et al.*, Correlation Between Kinetic-Energy Transfer to Rotation and to Phonons in Gas-Surface Collisions of NO with Ag(111), *Phys. Rev. Lett.*, 1986, **57**(16), 2053–2056.
21 C. T. Rettner, J. Kimman and D. J. Auerbach, Inelastic scattering of NO from Ag(111): Internal state, angle, and velocity resolved measurements, *J. Chem. Phys.*, 1991, **94**(1), 734–750.
22 F. H. Geuzebroek, *et al.*, Rotational excitation of oriented molecules as a probe of molecule-surface interaction, *J. Phys. Chem.*, 1991, **95**(21), 8409–8421.
23 K. R. Lykke and B. D. Kay, Rotational rainbows in the inelastic scattering of N_2 from Au(111), *J. Phys.: Condens. Matter*, 1991, **3**(suppl), S65.
24 K. R. Lykke and B. D. Kay, Rotationally inelastic gas–surface scattering: HCl from Au(111), *J. Chem. Phys.*, 1990, **92**(4), 2614–2623.
25 K. Golibrzuch, *et al.*, State-to-State Time-of-Flight Measurements of NO Scattering from Au(111): Direct Observation of Translation-to-Vibration Coupling in Electronically Nonadiabatic Energy Transfer, *J. Phys. Chem. A*, 2013, **117**(36), 8750–8760.
26 I. Rahinov, *et al.*, Efficient vibrational and translational excitations of a solid metal surface: State-to-state time-of-flight measurements of HCl(v = 2, J = 1) scattering from Au(111), *J. Chem. Phys.*, 2008, **129**(21), 214708.
27 Q. Ran, *et al.*, An advanced molecule-surface scattering instrument for study of vibrational energy transfer in gas-solid collisions, *Rev. Sci. Instrum.*, 2007, **78**(10), 104104.
28 B. Baule, Theoretische Behandlung der Erscheinungen in verdünnten Gasen, *Ann. Phys.*, 1914, **349**(9), 145–176.
29 R. Cooper, *et al.*, On the determination of absolute vibrational excitation probabilities in molecule-surface scattering: Case study of NO on Au(111), *J. Chem. Phys.*, 2012, **137**(6), 064705.
30 K. Golibrzuch, *et al.*, Experimental and Theoretical Study of Multi-Quantum Vibrational Excitation: NO(v = 0 → 1,2,3) in Collisions with Au(111), *J. Phys. Chem. A*, 2013, **117**(32), 7091–7101.
31 J. LaRue, *et al.*, Vibrationally promoted electron emission at a metal surface: electron kinetic energy distributions, *Phys. Chem. Chem. Phys.*, 2011, **13**(1), 97–99.
32 N. H. Nahler, *et al.*, Inverse Velocity Dependence of Vibrationally Promoted Electron Emission from a Metal Surface, *Science*, 2008, **321**(5893), 1191–1194.
33 J. D. White, *et al.*, Conversion of large-amplitude vibration to electron excitation at a metal surface, *Nature*, 2005, **433**(7025), 503–505.
34 F. Budde, *et al.*, State-resolved investigation of the dynamics of scattering and formation of NO at Ge surfaces, *Surf. Sci.*, 1987, **192**(2–3), 507–528.
35 G. O. Sitz, A. C. Kummel and R. N. Zare, Direct inelastic scattering of N_2 from Ag(111). I. Rotational populations and alignment, *J. Chem. Phys.*, 1988, **89**(4), 2558–2571.
36 J. L. W. Siders and G. O. Sitz, Observation and characterization of direct inelastic and trapping-desorption channels in the scattering of N_2 from Cu(110), *J. Chem. Phys.*, 1994, **101**(7), 6264–6270.